Research Article | Open Access

Soft Science

Sun *et al. Soft Sci.* **2026**, *6*, 43 **DOI:**10.20517/ss.2026.33

Self-stratified stretchable passive cooling interface for thermal management of on-skin electronics

Jiahao Sun[1,#], Mingzi Liu[2,#], Cancheng Jiang[3,#], Qingqiao Cai[1], Rong Cai[1], Jiahui Li[1], Yawen Xiao[1], Qingyi Xian[1], Xiaonan Sun[1], Lelun Jiang[1], Cheng Li[4], Chi Yan Tso[3], Xinge Yu[2], Yingying Zhou[5,*], Zehua Peng[1,*], Jiyu Li[1,*]

Keywords:
Passive cooling interface, liquid metal, radiative cooling, flexible electronics, thermal management, photoplethysmography

Citation: Sun, J.; Liu, M.; Jiang, C.; Cai, Q.; Cai, R.; Li, J.; Xiao, Y.; Xian, Q.; Sun, X.; Jiang, L.; Li, C.; Tso, C. Y.; Yu, X.; Zhou, Y.; Peng, Z.; Li, J. Self-stratified stretchable passive cooling interface for thermal management of on-skin electronics. *Soft Sci.* **2026**, *6*, 43. https://dx.doi.org/10.20517/ss.2026.33

Received: 9 Feb 2026 **First Decision:** 19 Mar 2026 **Revised:** 2 Apr 2026 **Accepted:** 24 Apr 2026 **Published:** 25 May 2026

Academic Editor: Kuniharu Takei **Copy Editor:** Xing-Yue Zhang **Production Editor:** Xing-Yue Zhang

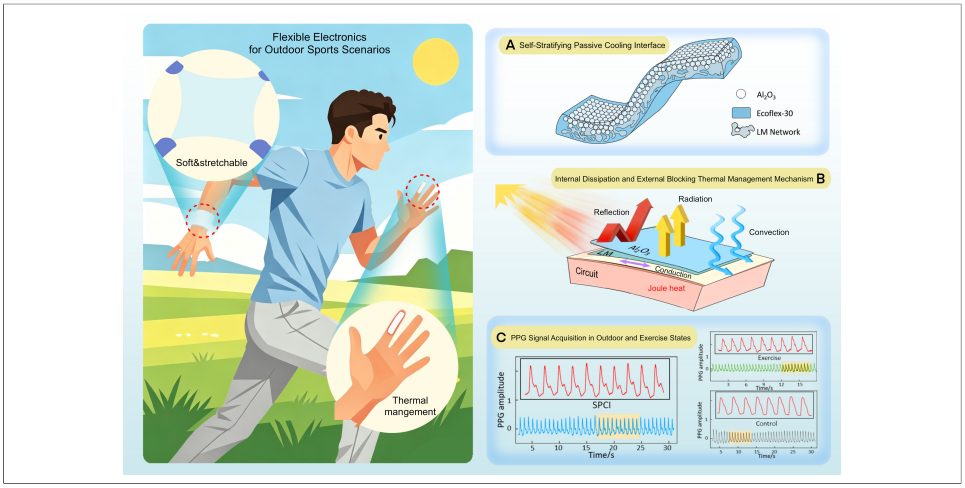

Abstract

Heat accumulation from Joule heating and solar irradiation severely challenges thermal safety and signal stability of long-term, outdoor on-skin electronics and human-machine interfaces. Here, we develop a self-stratified stretchable passive cooling interface (SPCI) that implements a synergistic internal-dissipation and external-blocking strategy by inducing gradient stratification via the density mismatch between Al_2O_3 microparticles and liquid metal (LM) within the elastomer. This mismatch triggers spontaneous self-stratification upon curing, yielding a multi-layer composite that features an Al_2O_3-enriched top layer for high solar reflectance (92.6%) and an LM-network-enriched bottom layer for efficient heat dissipation (thermal conductivity ≈ 1.5 $W \cdot m^{-1} \cdot K^{-1}$), while retaining soft mechanics (elastic modulus ≈ 0.082 MPa) and high stretchability (> 800% elongation). The SPCI exhibits excellent cooling performance in serpentine circuits at

[1]School of Biomedical Engineering, Shenzhen Campus of Sun Yat-sen University, Shenzhen 518107, Guangdong, China.
[2]Department of Biomedical Engineering, City University of Hong Kong, Hong Kong 999077, China.
[3]School of Energy and Environment, City University of Hong Kong, Hong Kong 999077, China.
[4]School of Chemical Engineering and Technology, Sun Yat-sen University, Zhuhai 519082, Guangdong, China.
[5]School of Professional Education and Executive Development, The Hong Kong Polytechnic University (PolyU SPEED), Hong Kong 999077, China.
[#]Authors contributed equally.

[*]**Correspondence to:** Dr. Jiyu Li, Dr. Zehua Peng, School of Biomedical Engineering, Shenzhen Campus of Sun Yat-sen University, Shenzhen 518107, Guangdong, China. E-mail: lijy887@mail.sysu.edu.cn; pengzeh@mail.sysu.edu.cn; Dr. Yingying Zhou, School of Professional Education and Executive Development, The Hong Kong Polytechnic University (PolyU SPEED), Hong Kong 999077, China. E-mail: july.zhou@cpce-polyu.edu.hk

200 mW, reducing peak temperature by up to 8.4 °C indoors and 12 °C outdoors under solar exposure, while maintaining effective cooling under tension. When integrated into a wireless skin-interfaced photoplethysmography platform for heart-rate monitoring, it lowers the maximum surface temperature by 8.6 °C during outdoor operation, enabling superior preservation of pulse-wave features compared with conventional elastomer encapsulation. This work establishes a scalable, mechanically compliant encapsulation interface for simultaneously mitigating internal and external thermal loads in wearable electronics and human-machine interfaces.

INTRODUCTION

Wearable devices are increasingly evolving toward "skin-like" electronics that integrate directly with human skin in an ultrathin, compliant, and conformal form, enabling long-term, low-burden on-body monitoring and human-machine interaction[1-5]. With continued advances in soft materials, device miniaturization, and system-level integration[6,7], skin-interfaced electronics are achieving higher functional density and increasing operational complexity, bringing their overall performance closer to that of conventional rigid electronics[8,9]. As wearable systems incorporate AI-assisted functions and increasingly multimodal processing[10,11], there is a concomitant rise in their power consumption and heat generation. Excessive temperature at the device's interface not only compromises wearing comfort and thermal safety[12,13], but also degrades the fidelity of acquired physiological signals, thereby limiting reliable long-term use in real-world settings[14]. The thermal load in wearable devices arises from two primary sources: internal Joule heat generated from circuits or components during operation and external heat influx from solar irradiation and ambient temperature[14-17]. However, effective thermal management remains a critical bottleneck for practical deployment as conventional approaches are often bulky and rigid, and may require additional energy input, making them incompatible with soft, skin-conformal wearables. Therefore, developing wearable-compatible encapsulation strategies that regulate the internal and external thermal loads while simultaneously preserving softness, stretchability and conformal contact is essential for ensuring safety and reliability during outdoor and long-term operation.

For the thermal management, especially under outdoor real-world conditions, passive radiative cooling, particularly daytime radiative cooling, has attracted extensive attention as it enables cooling without external energy input. Specifically, this cooling approach hinges on a dual-spectral selectivity mechanism: high reflectivity in the solar spectrum (0.3-2.5 μm) to minimize radiative heat absorption, and high emissivity within the atmospheric mid-infrared window (8-13 μm) to maximize radiative heat emission to outer space[18]. Radiative-cooling materials have demonstrated promise in outdoor applications such as buildings and transportation[19,20], and recent efforts have extended this concept to wearable electronics operating under sunlight[21-23]. Under outdoor conditions, particularly during daytime on-body use-high solar reflectance becomes even more critical for device thermal management by minimizing radiative heat gain from sunlight. Recently, radiative-cooling layers designed for wearables are often limited by suboptimal spectral selectivity and insufficient stretchability, and in most cases serve merely as passive "surface optical coatings" that only block solar irradiation[18]. A mature, skin-compatible encapsulation strategy capable of simultaneously dissipating internal Joule heat to the surroundings while blocking external radiative heat gain is still lacking, as internal Joule heating and solar irradiation often coexist in practical on-body scenarios[14,21,24]. These critical technical gaps underscore the need for developing flexible encapsulation systems that integrate efficient non-radiative heat dissipation with superior spectral performance, and can be seamlessly and scalably integrated with on-skin electronics to preserve thermal safety, stretchability and signal stability during prolonged outdoor on-body operation.

Conventional thermal management strategies for mitigating internal Joule heat in wearable electronics rely predominantly on enhancing thermal conduction and convection[12,25]; however, the incorporation of heat sinks or active cooling modules inevitably increases device volume, weight, and power consumption, which

conflicts with the requirements of skin-interfaced systems for lightweight, soft, and conformal form factors[26,27]. Another alternative strategy is to enhance the thermal conductivity of interface materials to construct in-plane heat-dissipation pathways[28,29], yet the most widely used elastomeric encapsulants[30,31] (e.g., polydimethylsiloxane and Ecoflex) possess intrinsically low thermal conductivity. While incorporating rigid fillers with high thermal conductivity into these materials can improve thermal conduction efficiency, this approach often compromises their stretchability, conformability, and processability, and may even lead to poor interfacial contact under repeated mechanical deformation[32,33]. Liquid metal (LM)-elastomer composites represent a promising solution: the intrinsically fluidic and reconfigurable metallic phase forms heat dissipation networks, thus substantially enhancing effective thermal conductivity and heat dissipation capability while preserving excellent mechanical properties[29,34]. However, existing LM-based thermal management strategies primarily target hotspots induced by internal Joule heat, and offer only limited mitigation of external thermal loads such as solar irradiation. In addition, practical implementation challenges, including leakage risk, the need for electrical insulation, and scalable integration with device packaging, continue to impede their widespread adoption in wearables and human-machine interfaces[35,36].

Here, we develop a self-stratified stretchable passive cooling interface (SPCI) based on an elastomer composite (Ecoflex-30) containing Al_2O_3 microparticles and LM, where the density mismatch between the two fillers drives spontaneous self-stratification during curing to form a gradient-stratified bilayer structure. Leveraging this self-stratifying material system, we propose an encapsulation-based thermal management strategy with an internal-dissipation and external-blocking mechanism for outdoor and long-term wearable applications. This design enables simultaneous regulation of internal and external thermal loads while maintaining excellent stretchability and mechanical compliance. The effectiveness of SPCI is validated through systematic material characterization, thermal analysis, and integration into a wearable PPG system.

EXPERIMENTAL

Optimization of Al_2O_3 particle size by numerical simulation

In this work, we designed a highly reflective encapsulation material by incorporating Al_2O_3 particles into an elastomer matrix. While the particle size of Al_2O_3 has a pronounced influence on the optical response of the elastomeric composite, we conducted the numerical simulation and calculations on the Al_2O_3 particles' scattering behavior using MATLAB to evaluate the effect of Al_2O_3 filler size on the optical performance and thereby guide the design of high-reflectance materials. Based on Mie scattering theory, Al_2O_3 particles were approximated as spherical scatterers dispersed within the elastomeric medium. The wavelength-dependent optical constants (refractive index) of Al_2O_3 in the target spectral range, together with the refractive index of the matrix, were used as inputs to calculate the scattering efficiency for particles with different diameters (d), thereby determining the optimal size. Details of the optical parameters and simulation settings have been added in Supplementary Materials S1. The reflectance spectra were further estimated using a Monte Carlo approach, where scattering contributions were weighted according to the solar spectrum over the relevant bands to obtain the theoretical reflectance trends as a function of particle size.

Fabrication of SPCI

Ecoflex-30 (Smooth-On; Ecoflex 00-30, 1.04 $g \cdot cm^{-3}$) was used as the elastomeric matrix. Functional fillers, including Al_2O_3 particles (500 nm, 3.95 $g \cdot cm^{-3}$; Changzhou Kenada New Materials) and a gallium-indium LM alloy (6.28 $g \cdot cm^{-3}$, melting point ≈ 16 °C; Dongguan Dingguan Metal Technology Co., Ltd.), were incorporated to prepare the encapsulation composite. Briefly, 5 g of Ecoflex-30 Part A and 5 g of Part B were added to a beaker, followed by the addition of dried Al_2O_3 powder and LM droplets (the masses were adjusted according to the target mass fractions; the mass ratios of liquid metal to Ecoflex-30 of 1:5, 2:5, and 3:5 correspond to mass fractions of 20%, 40%, and 60%, respectively. In this work, both the Al_2O_3 content and the LM content were defined with respect to the mass of the Ecoflex-30). Owing to surface tension and

density differences, the LM droplets tended to agglomerate and settle at the bottom. To obtain a homogeneous precursor, the mixture was mechanically stirred for 3 min to uniformly disperse the Al_2O_3 particles and LM droplets throughout the elastomer, yielding a composite slurry. The slurry was then degassed under vacuum for 2 min to remove trapped air bubbles. The degassed slurry was poured onto a glass substrate (70 mm × 70 mm × 1 mm) pre-coated with a mold-release agent and spin-coated at 120 revolutions per minute (rpm). To achieve the desired optical and thermal performance, the LM phase should be preferentially distributed toward the bottom region, with minimal LM present at the top surface. Therefore, sufficient curing time was provided, and the spin-coated samples were cured at 4 °C in a refrigerator for 3 hours. Based on calculations using Stokes' law [Supplementary Materials S2], the sedimentation distance of the liquid metal is matched to the film thickness, and the sedimentation time is synchronized with the curing time. As a result, sedimentation occurs concurrently with crosslinking, ultimately yielding a self-stratified structure. During 100 heating-cooling cycles (200 mW), the stability of the cooling performance was evaluated for three samples at intervals of every 20 cycles. After 1,000 cyclic stretching cycles (50%), the emissivity and cooling performance of the SPCI were measured, with the stability of the cooling performance for three samples assessed at intervals of every 200 cycles.

Fabrication of serpentine circuits and device integration

Serpentine circuits were designed using computer-aided drafting software (AutoCAD). The designed patterns were transferred onto PI/Cu laminates via laser cutting to achieve patterning, yielding a PI/Cu serpentine circuit [Supplementary Figure 1]. Specifically, a thin Ecoflex-30 base layer was first spin-coated onto a glass substrate pre-coated with a mold-release agent (Curing time was 60 s at 400 rpm and 60 ℃). The as-patterned serpentine circuit was then transfer-printed onto the Ecoflex-30 base layer. To avoid potential electrical shorting caused by direct contact between the LM and the circuit, an additional Ecoflex-30 insulation layer (100 μm) was spin-coated to fully encapsulate the serpentine conductor. Subsequently, the SPCI layer was integrated on top of the pre-encapsulated circuit to form the final thermally managed device.

Characterization

The optical properties of the SPCI were characterized by measuring its reflectance and emissivity spectra using a UV-vis-NIR spectrophotometer equipped with an integrating sphere (Agilent Technologies, Cary 5000) and a Fourier-transform infrared (FTIR) spectrometer (Bruker, Vertex 70), respectively. The surface morphology of the Al_2O_3 particles was examined by scanning electron microscopy (SEM; FEI Nova Nano SEM 450). The cross-sectional morphology of the SPCI was inspected by optical microscopy to evaluate the spatial distribution of the LM phase. The tensile properties were measured using a computer-controlled universal testing machine (SANS Testing Machine Co., Ltd., FBUTM6104). Temperature measurements were performed using infrared thermal cameras (FLUKE Ti400+ and FLIR A600-Series) and a thermocouple thermometer (YET-640), as specified for each experiment. Temperature measurements of all samples were performed at the back surface. All measured surfaces were made of uniform Ecoflex-30, so the emissivity of the FLUKE Ti400+ and FLIR A600 infrared thermometers was set to 0.95. The temperature results were verified by thermocouples [Supplementary Figure 2]. We measured the thermal conductivity of the SPCI using a thermal conductivity analyzer (DZDR-S, Nanjing Dazhan Instrument Co., Ltd.). The detailed test procedures and parameters are as follows: SPCI samples were fabricated into a uniform cuboid shape with the geometry of 4 cm × 4 cm × 0.8 cm, ensuring consistent thickness and flat surface to eliminate measurement errors caused by irregular sample morphology. To improve the reliability and repeatability of the test results, each sample was measured independently three times under the same experimental conditions, and the standard deviation of the three parallel measurements was recorded to reflect the stability of the test data. During the measurement, the heating plate of the thermal conductivity analyzer was clamped between two identical SPCI samples to achieve close contact between the sample and the heating plate, which effectively minimized the contact thermal resistance and ensured the accuracy of the measured thermal conductivity value.

Volunteer tests

The tests with volunteers are performed in compliance with ethical regulations under a protocol approved by the ethical committee of the Sun Yat-sen University (project license number JS-2025-249-01). All volunteers provided written informed consent at the time of recruitment.

RESULTS AND DISCUSSION

SPCI for thermal management in flexible electronics

To enable efficient thermal management for wearable and flexible electronic devices, we designed and fabricated a passive thermal-management interface in which functionally distinct layers spontaneously formed within a single elastomer composite, as schematically illustrated in Figure 1A. This self-stratified architecture provides an integrated thermal-management mechanism of internal heat dissipation and external heat blocking, thereby suppressing external heat input while facilitating the removal of internally generated heat. By exploiting the density mismatch between Al_2O_3 and LM, the SPCI spontaneously forms a self-stratified structure. Specifically, the SPCI comprises three layers: a top elastomer composite layer enriched with Al_2O_3 powder, a composition-gradient transition layer, and a bottom elastomer composite layer enriched with an interconnected LM network. The Al_2O_3 rich top layer affords high solar reflectance and mid-infrared emissivity, which is beneficial for radiative cooling, whereas the LM-network-rich bottom layer exhibits high thermal conductivity and promotes efficient interfacial heat transfer and in-plane heat dissipation.

The appearance of the SPCI is shown in Figure 1B. The front side [Figure 1B, left] is white and opaque, primarily due to strong visible-light scattering by Al_2O_3 particles. The back side [Figure 1B, right] reveals the preferential distribution of LM in the bottom region. In addition, the SPCI exhibits excellent stretchability. The SPCI can be seamlessly integrated with flexible circuits, as illustrated in Figure 1C. To prevent direct contact between the circuit and skin and to reduce the risk of short circuits caused by potential LM leakage, the flexible circuit is first fully pre-encapsulated with an elastomer to form an electrically insulating and biocompatible barrier. The SPCI is then integrated onto the pre-encapsulated circuit via a spin-coating process[3], yielding an integrated device that simultaneously provides thermal management as well as electrical and mechanical protection.

The thermal management mechanism based on the internal dissipation-external blocking concept is illustrated in Figure 1D. During operation, Joule heat generated in the circuit layer is first transferred through the interface to the heat-dissipation layer (the LM network enriched layer), where its high thermal conductivity enables rapid in-plane heat diffusion and temperature homogenization, thereby reducing local hotspots and suppressing heat accumulation. The heat is subsequently released to the surroundings through the encapsulation, primarily via conduction to the ambient environment, radiative heat dissipation, and convective heat transfer. Meanwhile, the reflective/radiative layer (the Al_2O_3 enriched layer) strongly reflects incident solar radiation and dissipates heat through infrared emission, thereby reducing the additional thermal load induced by sunlight. The synergistic effects effectively suppress device temperature rise, enhancing wearability and minimizing the risk of overheating-related skin burns.

The SPCI is also compatible with a broad range of flexible circuit platforms and can accommodate diverse fabrication and patterning methods [Supplementary Figure 3]. For example, the SPCI can be integrated with doctor-bladed conductive patterns [Figure 1E], as well as with flexible circuits obtained by laser patterning of PI/Cu laminates followed by transfer printing [Figure 1F]. Collectively, these results indicate that the SPCI serves as a general thermal-management encapsulation scheme that is applicable to flexible circuits fabricated via different processes, offering scalability and manufacturing adaptability for flexible electronic devices.

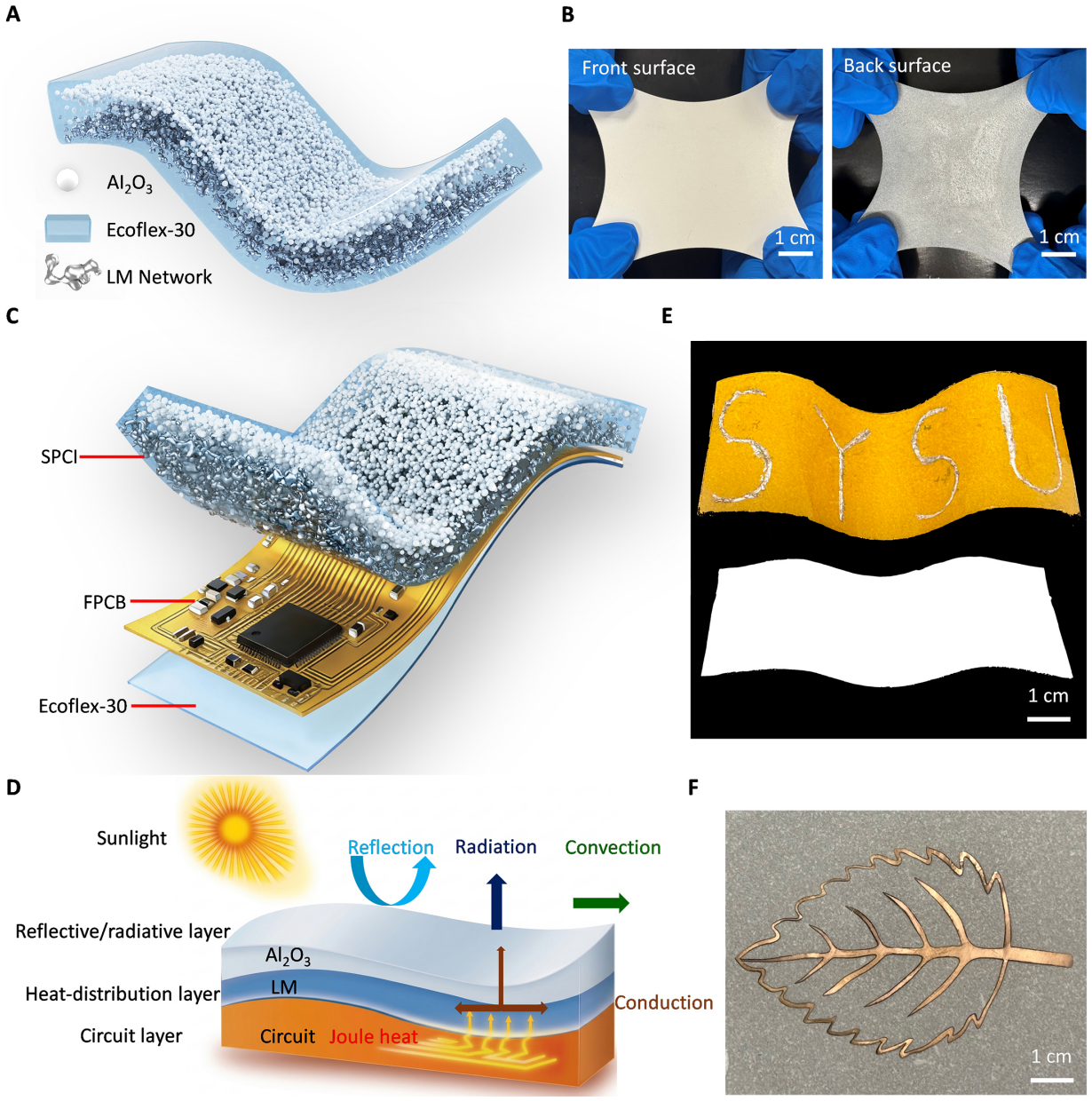

Figure 1. Overview of the SPCI and its applications. (A) Schematic illustration of the SPCI; (B) Photographs of the front and back sides of SPCI; (C) Schematic illustration of SPCI integrated with a flexible circuit; (D) Schematic of the "internal dissipation-external blocking" thermal-management mechanism; (E) Photograph of SPCI integrated with a blade-coated circuit (The top is the back view, and the bottom is the front view); (F) Photograph of SPCI integrated with a PI/Cu circuit. Photographed by the authors. SPCI: Stretchable passive cooling interface; PI: polyimide; LM: liquid metal; FPCB: flexible printed circuit board.

Fabrication and characterization of SPCI

As shown in Figure 2A, serpentine circuits were fabricated by first importing the designed serpentine-resistor pattern into a laser microfabrication system, followed by laser cutting to pattern PI/Cu laminates and obtain the serpentine conductor. The patterned circuit was then pre-encapsulated with Ecoflex-30 to form an electrically insulating and biocompatible protection layer. In parallel, Al_2O_3 particles and LM were introduced into the Ecoflex-30 matrix as functional fillers. After thorough mechanical mixing, the composite slurry was vacuum-degassed to remove trapped bubbles, and subsequently spin-coated onto the pre-encapsulated circuit surface. The integrated device was obtained after curing. Notably, to promote pronounced phase stratification between Al_2O_3 particles and LM, the spin-coated samples were cured at 4 °C.

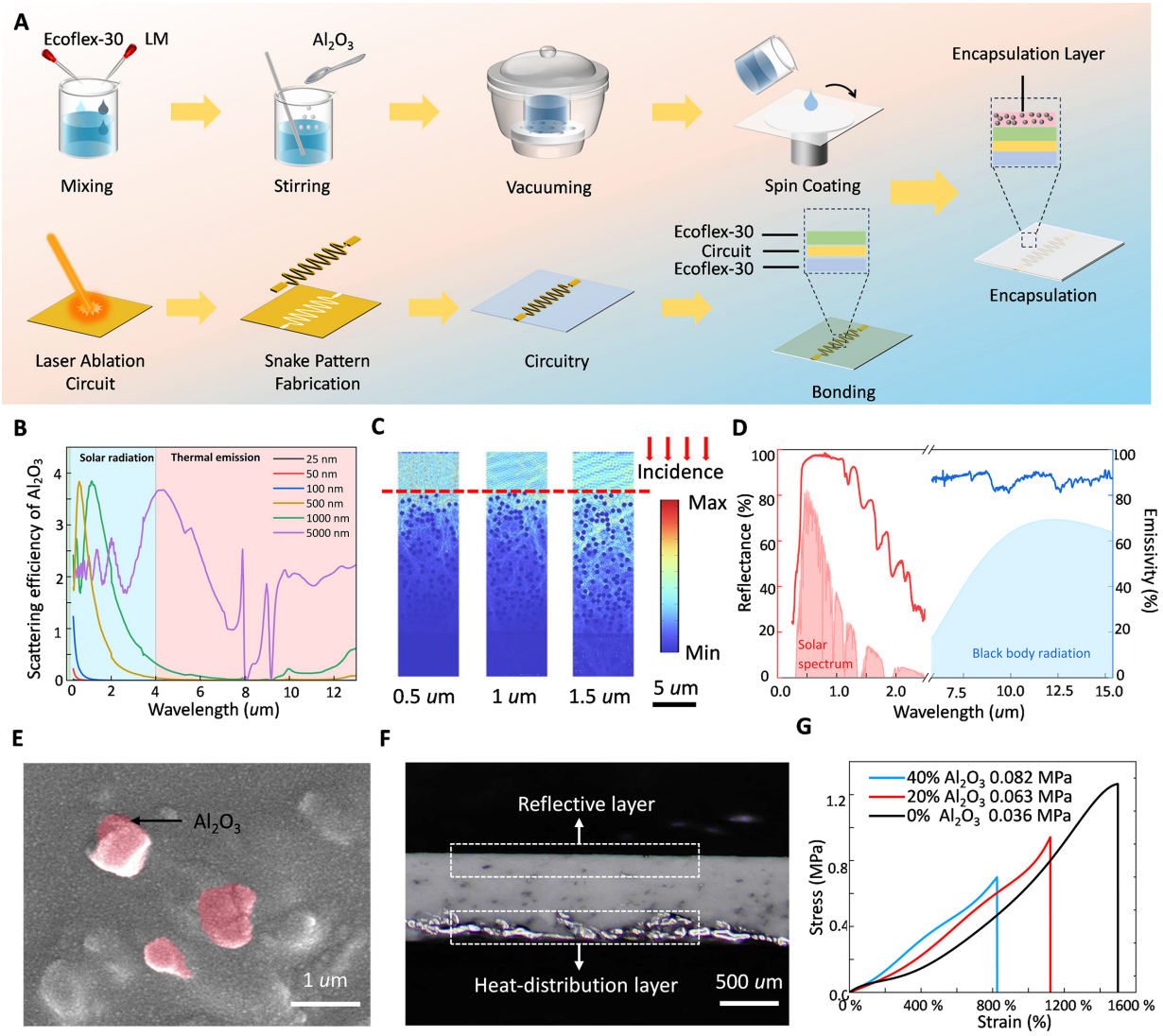

Figure 2. Fabrication and characterization of the SPCI. (A) Integration workflow of the SPCI with a serpentine-pattern circuit, including the fabrication of SPCI and the processing steps for the serpentine circuit; (B) Relationship between Al_2O_3 particle size and scattering efficiency; (C) Electromagnetic simulations of the electric-field distribution in SPCI under light illumination at wavelengths of 0.5, 1.0, and 1.5 μm; (D) Reflectance and emissivity spectra of SPCI (40 wt% Al_2O_3); (E) SEM image SPCI surface (Al_2O_3 particles are highlighted in pink); (F) Cross-sectional micrograph of SPCI; (G) Stress-strain curves of SPCI, showing the effect of varying Al_2O_3 loading ratios on tensile performance. Photographed by the authors. SPCI: Stretchable passive cooling interface; LM: liquid metal.

Because the Al_2O_3 particle size can significantly affect solar-light scattering, the scattering efficiency of Al_2O_3 with different diameters in the solar-irradiation and thermal-radiation bands was calculated based on Mie scattering theory [Figure 2B]. The results indicate that Al_2O_3 particles with a diameter of 500 nm provide stronger scattering in the visible-near-infrared range, which is favorable for enhancing solar reflectance. The electric-field distributions in Figure 2C further illustrate the propagation of incident light at different wavelengths, where light within the solar spectrum is substantially attenuated after penetrating several tens of micrometers, leading to efficient backscattering.

The measured spectral reflectance and emissivity of the SPCI are shown in Figure 2D. The sample (40 wt% Al_2O_3) exhibits high reflectance across the solar spectrum, with an average solar reflectance of 92.6%. Meanwhile, it maintains a high emissivity (mid-infrared emissivity 90%) in the mid-infrared region, particularly within the atmospheric window, outperforming common flexible encapsulation substrates (e.g.,

PDMS[37]) in thermal management related optical responses, thereby supporting its radiative-cooling potential. In terms of microstructure, SEM images reveal that Al_2O_3 particles are uniformly dispersed within the elastomeric matrix [Figure 2E, pink-labeled regions]. The film thickness, measured by a vernier caliper, is approximately 600 μm. Cross-sectional optical microscopy further confirms the self-stratified three-layer architecture of the SPCI [Figure 2F], consisting of an Al_2O_3-enriched reflective/emissive top layer and an LM-enriched bottom layer forming a continuous, percolated network that enables high effective thermal conductivity and enhanced in-plane heat dissipation. Given the stretchability observed in the photographs [Figure 1B] and the requirements for on-body integration, the tensile properties of SPCIs with different Al_2O_3 loadings were evaluated (The SPCI was cut into a dumbbell-shaped specimen using a mold. Supplementary Figure 4). With increasing Al_2O_3 content, the elongation at break decreases while the elastic modulus increases. At 40 wt% Al_2O_3, the SPCI retains an elongation at break exceeding 800% [Figure 2G], which is substantially higher than the maximum strain generally experienced by human skin (< 50%)[38], while maintaining a low elastic modulus (0.082 MPa), thereby balancing thermal-management functionality with deformation tolerance. We also simulated and characterized the morphological stability of the liquid metal under stretching, as detailed in Supplementary Figures 5 and 6. Under 50% tensile strain, the liquid metal maintains continuous connectivity, forming effective thermal conduction pathways. Further increasing the Al_2O_3 loading markedly raises slurry viscosity and complicates film formation, narrowing the processing window and hindering robust fabrication and device integration. The SPCI also exhibited good biocompatibility [Supplementary Figure 7] and long-term stability. After 1000 cycles of stretching and 100 heating-cooling cycles, the optical properties were well preserved, with both solar reflectance and infrared emissivity remaining at ~92% of their initial values [Supplementary Figure 8]. The thermal-management performance also showed minimal variation, with a change of only ~5% [Supplementary Figure 9]. In addition, the adhesion stability between the pre-encapsulated circuit and the SPCI is 12 N/cm, the results demonstrate the mechanical robustness and reliability of the system. Compared with recent flexible/stretchable radiative cooling materials, SPCI exhibits excellent spectral performance and stretchability [Supplementary Table 1].

Cooling performance of SPCI

Because Joule heat generated by electronic components is a primary cause of temperature rise in electronic devices[39,40], we employed a representative serpentine resistor as a standardized heating element to evaluate the heat-dissipation capability of the SPCI based on the internal dissipation-external blocking mechanism. The cooling performance of the SPCI arises from the synergistic coupling of solar reflection, internal heat transport, radiative emission, and convective heat transfer. Under solar irradiation, the Al_2O_3 enriched top layer suppresses heat gain by strongly reflecting incident sunlight, while under indoor or Joule-heating conditions, the liquid-metal (LM) network facilitates efficient internal heat spreading and removal. Supplementary Figure 10 further shows that solar absorption is markedly reduced in the SPCI, whereas heat dissipation is dominated by convection, with radiation providing an additional contribution. Control experiments confirm that the Al_2O_3 layer mainly reduces external solar heat input, while the LM network governs internal heat transport and overall heat dissipation; their integration therefore yields substantially greater passive cooling than either component alone [Supplementary Figure 11]. In contrast to conventional elastomer encapsulation, which lacks both high solar reflectivity and efficient thermal conduction, the SPCI integrates heat blocking, heat spreading, and heat dissipation within a single architecture. Following the fabrication procedure in Figure 2A, the serpentine heater was encapsulated between an elastomer substrate and the SPCI [Figure 3A], where the left and right panels show the front and back views of the device, respectively. The serpentine heater and the SPCI maintain conformal contact and structural integrity under stretching, folding, twisting, and hand-mounted integration [Figure 3B], demonstrating the deformation adaptability required for flexible-electronics applications. We evaluated the stability of the insulating layer by measuring the resistance [Supplementary Figure 12] between the SPCI and the circuit and by optical imaging

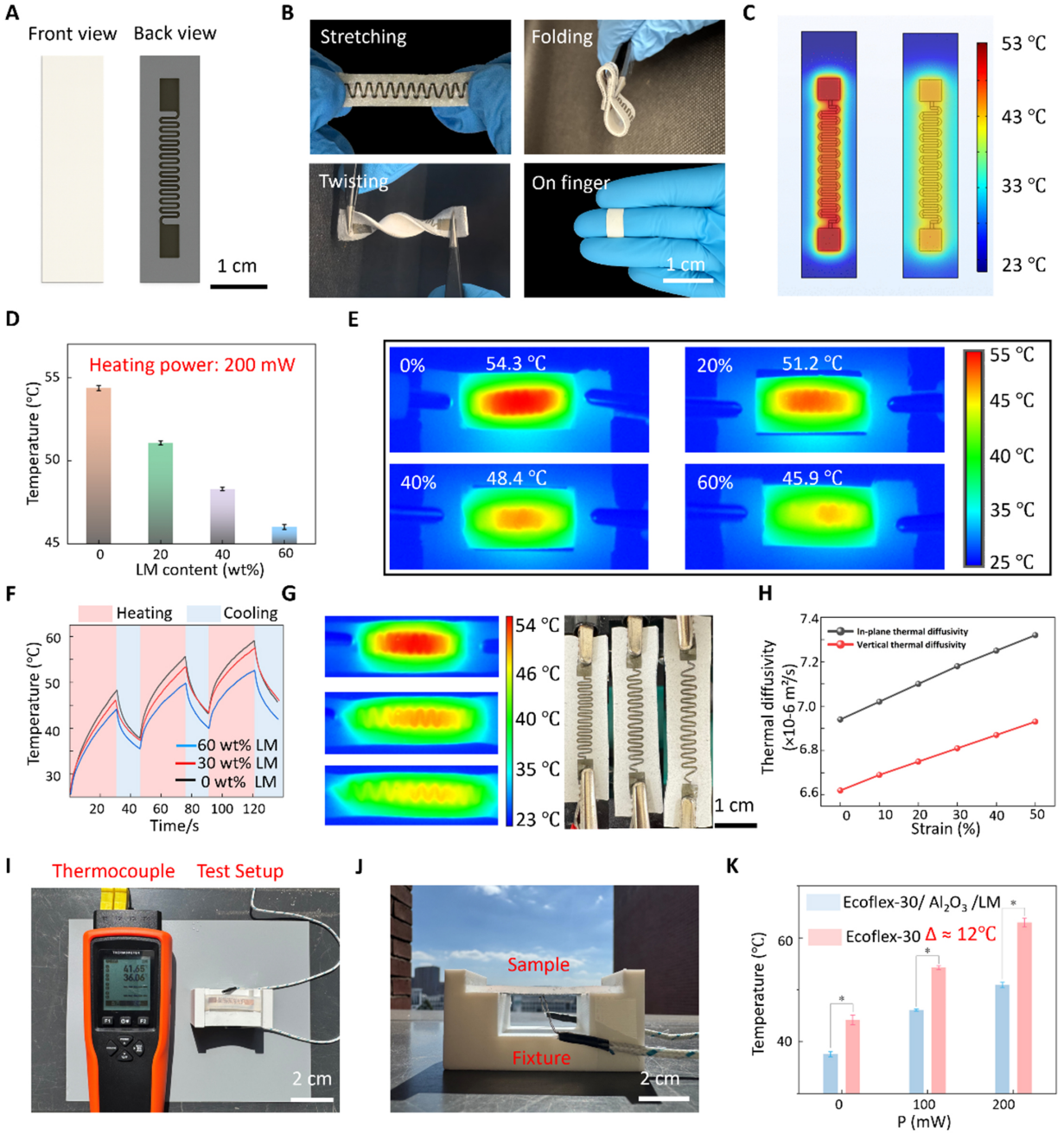

Figure 3. Device integration and cooling performance. (A) Front-and back-side photographs of SPCI integrated with a serpentine resistive heater; (B) Photographs showing conformal and robust attachment of SPCI-serpentine circuit assembly under stretching, folding, twisting, and on-hand mounting conditions; (C) Temperature distributions of serpentine circuits encapsulated with Ecoflex-30 (left) and with SPCI containing a 60 wt% LM (right); (D) Cooling performance of serpentine circuits with different LM mass fractions under a heating power of 200 mW; (E) Infrared thermography images of the serpentine circuit corresponding to (D); (F) Transient temperature profiles of serpentine circuits with different LM mass fractions under pulsed heating at 200 mW; (G) Infrared thermography images of the serpentine circuit under tensile deformation (top: original length, 3.0 cm; middle: stretched to 3.75 cm; bottom: stretched to 4.5 cm). The corresponding optical images under each tensile state are shown on the right; (H) Calculated equivalent thermal diffusivity coefficient; (I) and (J) Schematic illustration of the outdoor temperature-measurement setup (Cooling performance during 14 October, 11:00-13:00, Shenzhen, China); (K) Outdoor cooling performance of the serpentine circuit under different heating powers. Photographed by the authors. SPCI: Stretchable passive cooling interface; LM: liquid metal.

[Supplementary Figure 13]. The results demonstrate that the SPCI exhibits low risk of liquid metal leakage and maintains reliable electrical insulation.

We first investigated the performance of the SPCI for dissipating internally generated heat [Figure 3C-H]. Temperature-field simulations were conducted to compare the steady-state temperature distributions of serpentine heaters under different encapsulation conditions [Figure 3C]. At the same input power (200 mW), the SPCI used in this work (40 wt% Al_2O_3 and 60 wt% LM) substantially reduced the heater temperature relative to the Ecoflex-30 encapsulated control with the same overall thickness, with a simulated temperature reduction of ~8 °C. The simulation details are provided in the Supplementary Materials S3. We then fabricated SPCIs with different LM contents and performed steady-state heating experiments (The testing setup is shown in Supplementary Figure 14). After thermal equilibrium was reached, the maximum device temperature decreased monotonically with increasing LM content [Figure 3D]. Consistently, infrared thermography [Figure 3E] shows that at 200 mW the peak temperature decreased from 54.3 °C for 0 wt% LM to 45.9 °C for 60 wt% LM, corresponding to a maximum temperature reduction of 8.4 °C, which is in good agreement with the simulation results. This is because, as the liquid metal content increases, the liquid-metal network in the bottom layer becomes progressively more continuous [Supplementary Figure 15], forming complete heat-conduction pathways that enable faster heat transfer and dissipation.

Considering that wearable flexible devices often operate intermittently (e.g., periodic activation for heart-rate and SpO_2 measurements)[41], we further applied pulsed heating to the serpentine circuits (200 mW, 30 s on/15 s off, repeated for three cycles) and obtained the temperature-time response [Figure 3F]. Compared with the control, encapsulation with LM-containing SPCI lowers the peak temperature during the heating stage and accelerates temperature decay during the cooling stage, thereby effectively suppressing temperature accumulation and fluctuations under cyclic operation, which is beneficial for long-term stable operation and wearing comfort. Under tensile deformation, the encapsulated device retains pronounced heat-dissipation capability [Figure 3G and H].

With increasing tensile strain, the temperature distribution becomes more uniform and the peak temperature further decreases. This behavior can be attributed to the increased effective heat-dissipation area and reduced heat flux per unit area upon stretching, while the LM heat dissipation network further promotes lateral heat diffusion and enhances convective and radiative heat loss to the environment. Subsequently, theoretical calculations were performed to analyze the anisotropic heat-transport behavior and thermal dissipation performance under different tensile strains [Figure 3H]. Simulation details are provided in the Supplementary Materials S4. The effective thermal conductivity was quantified over a strain range of 0%-50%, revealing how stretching modulates thermal management by altering the material thickness, effective area, and layered architecture. With increasing strain, the effective thermal diffusivity in both directions exhibits an upward trend: the in-plane enhancement arises from the enlarged effective heat-transfer area, whereas the vertical increase is attributed to the reduced composite thickness and shortened heat-transfer pathway.

Finally, to validate thermal management performance under outdoor conditions, we built a thermocouple-based measurement setup and a fixture for outdoor testing (Figure 3I and J, the solar irradiance was approximately 830 W/m², the ambient air temperature was 32 °C, and the wind speed was 2 m/s.), and compared two encapsulation schemes (pure Ecoflex-30 and SPCI containing 60 wt% LM). The thermocouple was placed on the device backside to represent the skin-contact-side temperature. The results show that SPCI-encapsulated serpentine heaters exhibit significantly lower steady-state temperature rise across different input powers [Figure 3K] at 200 mW, the backside temperature reduction reaches ~12 °C. This improvement arises from the combined effects of enhanced internal heat dissipation by the LM network and reduced external heat gain due to the reflective/emissive surface layer, leading to effective thermal management under outdoor conditions. Compared with recent studies on LM-elastomer composites[29,42-44], SPCI demonstrates advantages in spectral performance, maximum stretchability, and cooling power [Supplementary Figure 16].

SPCI-enabled enhanced PPG signal fidelity

In skin-interfaced human-machine interfaces and flexible wearable electronics, effective thermal management is essential for ensuring user comfort, safety, and signal stability. To validate the effectiveness of the internal dissipation-external blocking thermal-management strategy in realistic wearable scenarios, we designed and built a skin-conformal wireless PPG acquisition platform for real-time pulse-wave monitoring, and evaluated the impact of the SPCI on device temperature rise and signal quality [Figure 4A-H]. As shown in Figure 4A, the platform is implemented on a flexible printed circuit board (FPCB) and integrates a PPG sensing module, a microcontroller unit (MCU), a low-power Bluetooth module, a battery module, and associated discrete components, forming a standalone wireless acquisition system [Supplementary Figure 17].

The encapsulation configuration is illustrated in Figure 4B and C. The device front side is encapsulated with Ecoflex-30 to provide electrical insulation and a skin-isolation barrier, whereas the backside is integrated with the SPCI as the thermal management layer. This packaging maintains good compliance and structural integrity under bending [Figure 4C] and enables conformal integration on the hand skin surface [Figure 4D]. The adhesion strength (0.28 N/cm) between the device and the skin is comparable to that of commercially available 3M medical tape, indicating reliable and practical skin attachment [Supplementary Figure 18].

Outdoor continuous-operation tests were then conducted under natural environmental conditions, and the time-dependent surface temperature was recorded [Figure 4E]. Compared with the control device fully encapsulated with Ecoflex-30, the SPCI-integrated device exhibits a markedly reduced temperature rise and a substantially lower peak temperature. Corresponding infrared thermography (Figure 4F, the solar irradiance ≈ 780 W/m^2, ambient air temperature was 27 °C, and wind speed was 4 m/s) shows that the control reaches a maximum temperature of 42 °C, whereas the SPCI device peaks at 33.4 °C, yielding a maximum temperature difference of 8.6 °C.

The underlying mechanism is schematically illustrated in Figure 4G. The same thermal-management principle applies to the wearable PPG platform, resulting in reduced device temperature and improved signal fidelity.

The temperature reduction further translates into improved signal quality. As shown in Figure 4H, the SPCI-encapsulated device preserves clear pulse periodicity, stable amplitude, and identifiable dicrotic-notch features, whereas the control exhibits pronounced waveform distortion and loss of fine details[45,46]. Quantitatively, the dicrotic-notch identifiability index (Details of calculation have been added to Supplementary Materials S5) is only ~30% for the control, but exceeds 95% for the SPCI-encapsulated device, indicating much better preservation of physiologically relevant waveform features. Even under post-exercise conditions, the index remains > 80%, confirming robust signal fidelity under sweating and motion disturbance. Consistently, the SPCI-encapsulated device also shows a higher SNR (The SPCI group exhibits an SNR of 19 dB, compared with 6 dB for the control group and 16 dB for the SPCI group after exercise) than the control. These results demonstrate that SPCI not only reduces device temperature during on-body outdoor operation, but also improves the fidelity and robustness of continuous PPG monitoring. Previous reports have demonstrated that radiative-cooling or thermal-management layers can be integrated with wearable physiological sensing platforms to improve operational stability in outdoor environments, including patch-type tissue oximeters for stable optical sensing under sunlight[1] and wearable stress-monitoring electronics for outdoor workers[17]. In contrast to these device-specific cooling designs, our SPCI serves as an intrinsically stretchable encapsulation interface that simultaneously regulates internally

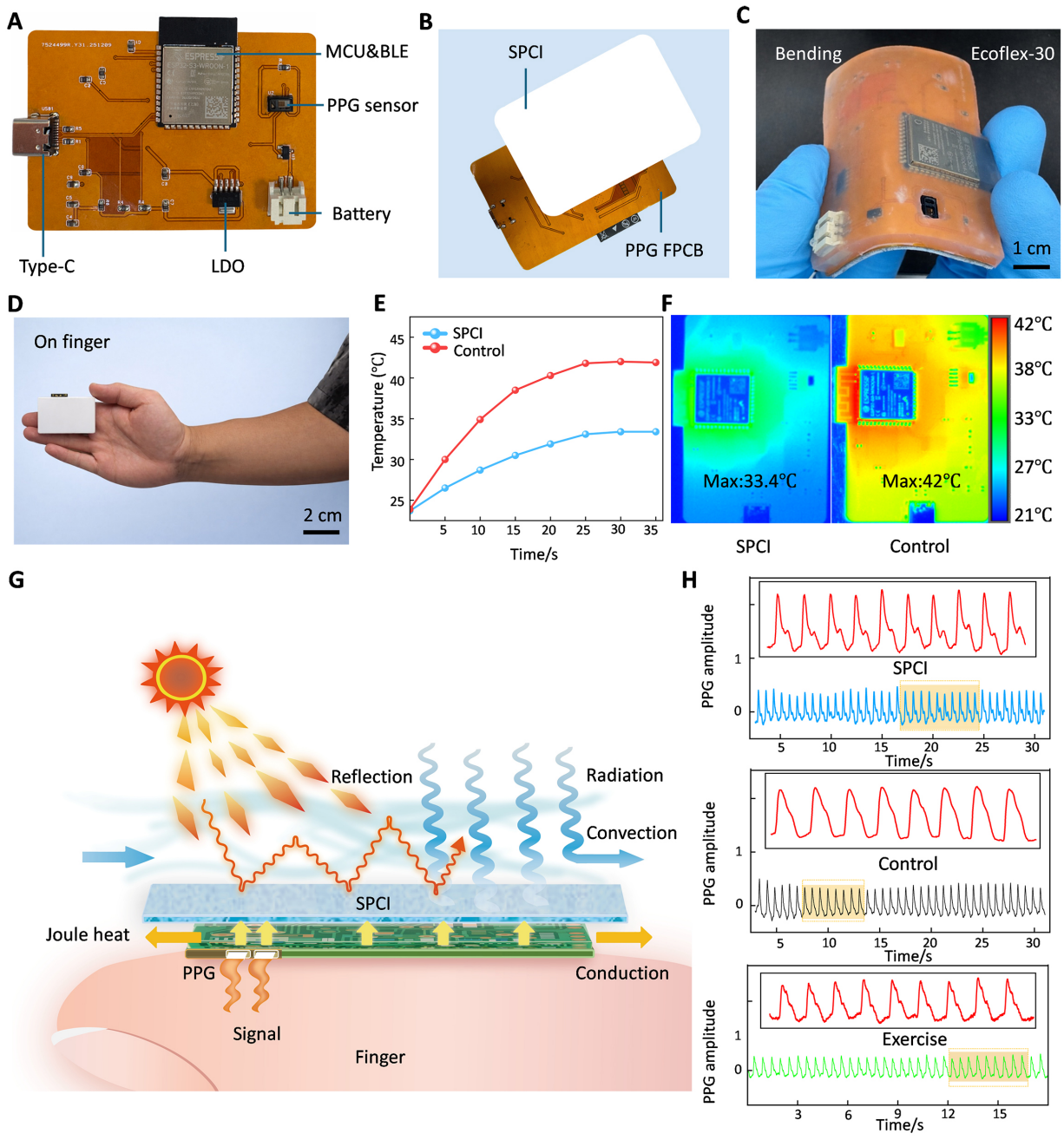

Figure 4. Improved fidelity of PPG physiological-signal acquisition enabled by SPCI. (A) Photograph of the PPG-sensing FPCB; (B) Exploded-view schematic of the encapsulated PPG device; (C) Photograph of the device under bending deformation; (D) Photograph of the device attached to a fingertip; (E) Device temperature evolution during continuous outdoor operation (control group: encapsulated with Ecoflex-30); (F) Corresponding infrared thermography images for (E) (Test during 3 November, 11:00-13:00, Shenzhen, China); (G) Schematic of thermal-exchange processes in the device; (H) Fingertip PPG signals corresponding to the conditions in (E) and (F). Photographed by the authors. SPCI: Stretchable passive cooling interface; PPG: photoplethysmography; FPCB: flexible printed circuit board; MCU: microcontroller unit; BLE: bluetooth low energy; LDO: low dropout regulator.

generated Joule heat and external solar heat gain. The improved preservation of fine PPG waveform features further supports the utility of this encapsulation strategy for outdoor wearable sensing.

Limitations and outlook

Despite the promising thermal-management performance of the SPCI, several limitations of this study should be acknowledged. First, although the outdoor tests and wearable demonstrations validated the feasibility of the proposed strategy, the evaluation was still limited to specific environmental conditions,

device configurations, and short-term use scenarios. Broader validation under diverse climates, longer wearing durations, and different types of wearable systems will be necessary to fully assess its practical robustness. Second, although the insulating encapsulation design reduced the risk of direct liquid-metal exposure and failure, the potential leakage issue of liquid metal has not been fully resolved, and its long-term safety and reliability under repeated deformation, sweating, and real-world use conditions still require further investigation. Third, the present work mainly focuses on proof-of-concept device integration, and future studies should further optimize large-area fabrication, encapsulation uniformity, and compatibility with more complex wearable electronics. In the future, these efforts may help establish SPCI as a scalable and versatile thermal-management platform for long-term outdoor wearable sensing and other soft electronic systems.

CONCLUSIONS

In summary, we have developed the SPCI for on-skin electronics and human-machine interfaces, enabling effective thermal management under simultaneous internal Joule heating and external thermal loading. In the field of wearable devices, SPCI can be integrated into smart clothing, wearable health monitors, and flexible heating or cooling equipment. Its soft and stretchable characteristics are compatible with human skin and body movements, while its efficient thermal conductivity enables rapid heat dissipation or temperature regulation, solving the core problem of poor thermal management in traditional wearable electronics. For flexible electronic devices such as flexible displays, stretchable sensors, and soft robots, SPCI can serve as a thermal management matrix, effectively reducing the operating temperature of electronic components, improving device stability and service life, and promoting the industrialization of flexible electronic technology. In terms of high-power electronic equipment, SPCI can be used as a thermal interface material for chips, LEDs, and power batteries, replacing traditional rigid thermal management materials. Its excellent thermal conductivity and interface adhesion ensure efficient heat transfer, while its flexibility can adapt to the irregular surfaces of electronic components, reducing contact thermal resistance and improving heat dissipation efficiency. Compared with existing liquid-metal-based thermal management materials, SPCI offers a simple preparation process, low cost, and low leakage risk. Together with its available and inexpensive raw materials, these advantages give it potential for scalable industrial production. Overall, this gradient-stratified bilayer encapsulation interface provides a scalable and versatile thermal-management solution for flexible wearable electronics exposed to both internal heat generation and external solar irradiation.

DECLARATIONS

Acknowledgements

The authors acknowledge the support from the University Grants Committee-Faculty Development Scheme-UGC/FDS24/M02/24.

Authors' contributions

Conceptualization, methodology, investigation, data acquisition and analysis, and the manuscript writing: Sun, J.; Liu, M.; Jiang, C.
Conceptualization: Cai, Q.; Cai, R.
Methodology: Li, J.; Sun, X.
Investigation: Xiao, Y.; Xian, Q.
Analyzed and discussed the results: Li, C.
Conceiving research protocol, supervising the overall work, providing resource support, and reviewing and editing the manuscript: Li, J.; Peng, Z.; Zhou, Y.; Yu, X.; Tso, C. Y.; Jiang, L.

Availability of data and materials

The original contributions presented in this study are included in the article/Supplementary Materials. Further inquiries can be directed to the corresponding author(s).

AI and AI-assisted tools statement

Not applicable.

Financial support and sponsorship

This work was supported by the Start-up Fund of Sun Yat-sen University (No. 76190-12255012), the National High-Level Young Talents Program (with provincial government matching research funds) (No. 76190-42150002) and Shenzhen Medical Research Special Fund Project (No. A2503033).

Conflicts of interest

Yu, X. is an Editorial Board Member of the journal *Soft Science* but is not involved in any steps of editorial processing, notably including reviewer selection, manuscript handling, or decision-making, while the other authors declared that they have no conflicts of interest.

Ethical approval and consent to participate

The tests with volunteers are performed in compliance with ethical regulations under a protocol approved by the ethical committee of the Sun Yat-sen University (project license number JS-2025-249-01). All volunteers provided written informed consent at the time of recruitment.

Consent for publication

Not applicable.

Supplementary Materials

Supplementary Materials

REFERENCES

1. Kang, M. H.; Lee, G. J.; Lee, J. H.; et al. Outdoor-useable, wireless/battery-free patch-type tissue oximeter with radiative cooling. *Adv. Sci.* **2021**, *8*, 2004885. DOI PubMed PMC
2. Xu, J.; Chen, X.; Li, S.; et al. On-skin epidermal electronics for next-generation health management. *Nano-Micro. Lett.* **2025**, *18*, 25. DOI PubMed PMC
3. Li, J.; Yang, P.; Li, X.; et al. Ultrathin smart energy-storage devices for skin-interfaced wearable electronics. *ACS. Energy. Lett.* **2022**, *8*, 1-8. DOI
4. Zarei, M.; Lee, G.; Lee, S. G.; Cho, K. Advances in biodegradable electronic skin: material progress and recent applications in sensing, robotics, and human-machine interfaces. *Adv. Mater.* **2022**, *35*, 2203193. DOI PubMed
5. Mao, P.; Li, H.; Yu, Z. A review of skin-wearable sensors for non-invasive health monitoring applications. *Sensors* **2023**, *23*, 3673. DOI PubMed PMC
6. Zhang, B.; Li, J.; Zhou, J.; et al. A three-dimensional liquid diode for soft, integrated permeable electronics. *Nature* **2024**, *628*, 84-92. DOI PubMed
7. Mohammadi, M.; Shang, J.; Li, Y.; et al. Miniaturized soft and stretchable multilayer circuits through laser-defined high aspect-ratio printing. *Small* **2025**, *21*, 2501175. DOI PubMed PMC
8. Yang, X.; Chen, W.; Fan, Q.; et al. Electronic skin for health monitoring systems: properties, functions, and applications. *Adv. Mater.* **2024**, *36*, 2402542. DOI PubMed
9. Mahato, K.; Saha, T.; Ding, S.; Sandhu, S. S.; Chang, A.; Wang, J. Hybrid multimodal wearable sensors for comprehensive health monitoring. *Nat. Electron.* **2024**, *7*, 735-50. DOI
10. Matsumura, G.; Honda, S.; Kikuchi, T.; et al. Real-time personal healthcare data analysis using edge computing for multimodal wearable sensors. *Device* **2025**, *3*, 100597. DOI
11. Song, Y.; Tay, R. Y.; Li, J.; et al. 3D-printed epifluidic electronic skin for machine learning-powered multimodal health surveillance. *Sci. Adv.* **2023**, *9*, eadi6492. DOI PubMed PMC
12. Yun, J. Recent progress in thermal management for flexible/wearable devices. *Soft. Sci.* **2023**, *3*, 12. DOI
13. Yoo, S.; Yang, T.; Park, M.; et al. Responsive materials and mechanisms as thermal safety systems for skin-interfaced electronic devices. *Nat. Commun.* **2023**, *14*, 1024. DOI PubMed PMC

14. Li, J.; Fu, Y.; Zhou, J.; et al. Ultrathin, soft, radiative cooling interfaces for advanced thermal management in skin electronics. *Sci. Adv.* **2023**, *9*, eadg1837. DOI PubMed PMC
15. Yu, H.; Zhang, S.; Lian, Y.; et al. Electronic textile with passive thermal management for outdoor health monitoring. *Adv. Fiber. Mater.* **2024**, *6*, 1241-52. DOI
16. Hyeon, C.; Jeong, M.; Kwon, S.; et al. Thermal protection of wearable devices under outdoor conditions using radiative cooling films. *Opt. Mater.* **2025**, *167*, 117258. DOI
17. Kim, H.; Yoo, Y. J.; Yun, J. H.; Heo, S. Y.; Song, Y. M.; Yeo, W. H. Outdoor worker stress monitoring electronics with nanofabric radiative cooler-based thermal management. *Adv. Healthc. Mater.* **2023**, *12*, 2301104. DOI PubMed
18. Xie, F.; Jin, W.; Nolen, J. R.; et al. Subambient daytime radiative cooling of vertical surfaces. *Science* **2024**, *386*, 788-94. DOI PubMed
19. Kousis, I.; Pisello, A. L. Toward the scaling up of daytime radiative coolers: a review. *Adv. Opt. Mater.* **2023**, *11*, 2300123. DOI
20. Xie, A. Q.; Qiu, H.; Jiang, W.; et al. Recent advances in spectrally selective daytime radiative cooling materials. *Nano-Micro. Lett.* **2025**, *17*, 264. DOI PubMed PMC
21. Dong, J.; Peng, Y.; Zhang, Y.; et al. Superelastic radiative cooling metafabric for comfortable epidermal electrophysiological monitoring. *Nano-Micro. Lett.* **2023**, *15*, 181. DOI PubMed PMC
22. Li, X.; Xie, Z.; Chen, B.; et al. Transparent radiative cooler with high thermal conductivity for heat dissipation in electronic devices. *Cell. Rep. Phys. Sci.* **2025**, *6*, 102505. DOI
23. Peng, Y.; Dong, J.; Zhang, Y.; et al. Thermally comfortable epidermal bioelectrodes based on ultrastretchable and passive radiative cooling e-textiles. *Nano. Energy.* **2024**, *120*, 109143. DOI
24. Jung, Y.; Kim, M.; Jeong, S.; Hong, S.; Ko, S. H. Strain-insensitive outdoor wearable electronics by thermally robust nanofibrous radiative cooler. *ACS. Nano.* **2024**, *18*, 2312-24. DOI PubMed
25. Dhumal, A. R.; Kulkarni, A. P.; Ambhore, N. H. A comprehensive review on thermal management of electronic devices. *J. Eng. Appl. Sci.* **2023**, *70*, 140. DOI
26. Zhu, Y.; Li, J.; Kim, J.; et al. Skin-interfaced electronics: a promising and intelligent paradigm for personalized healthcare. *Biomaterials* **2023**, *296*, 122075. DOI PubMed PMC
27. Choi, J.; Dun, C.; Forsythe, C.; Gordon, M. P.; Urban, J. J. Lightweight wearable thermoelectric cooler with rationally designed flexible heatsink consisting of phase-change material/graphite/silicone elastomer. *J. Mater. Chem. A.* **2021**, *9*, 15696-703. DOI
28. Chen, H.; Ding, Y.; Zhu, G.; et al. A new route to fabricate flexible, breathable composites with advanced thermal management capability for wearable electronics. *npj. Flex. Electron.* **2023**, *7*, 24. DOI
29. Li, X.; Lin, J.; Wu, J.; et al. Stretchable and leakage-free liquid metal networks for thermal management. *Adv. Funct. Mater.* **2025**, *35*, 2420839. DOI
30. Kim, S.; Kang, J.; Lee, I.; et al. An intrinsically stretchable multi-biochemical sensor for sweat analysis using photo-patternable ecoflex. *npj. Flex. Electron.* **2023**, *7*, 33. DOI
31. Wang, H.; Zhao, Z.; Liu, P.; Guo, X. A soft and stretchable electronics using laser-induced graphene on polyimide/PDMS composite substrate. *npj. Flex. Electron.* **2022**, *6*, 26. DOI
32. Zhu, H.; Wu, S.; Tang, R.; et al. DIW-printed thermal management PDMS composites with 3D structural thermal conductive network of h-BN platelets and Al_2O_3 nanoparticles. *Polymers* **2024**, *16*, 1491. DOI PubMed PMC
33. Zhang, X.; Song, J.; Meng, J.; Zhang, K. Anisotropic PDMS/Alumina/Carbon fiber composites with a high thermal conductivity and an electromagnetic interference shielding performance. *Materials* **2022**, *15*, 8078. DOI PubMed PMC
34. Bartlett, M. D.; Kazem, N.; Powell-palm, M. J.; et al. High thermal conductivity in soft elastomers with elongated liquid metal inclusions. *Proc. Natl. Acad. Sci. U.S.A.* **2017**, *114*, 2143-8. DOI PubMed PMC
35. Xu, Y.; Su, Y.; Xu, X.; et al. Porous liquid metal-elastomer composites with high leakage resistance and antimicrobial property for skin-interfaced bioelectronics. *Sci. Adv.* **2023**, *9*, eadf0575. DOI PubMed PMC
36. Yang, X.; Liu, H.; Pan, T.; Li, B.; Chu, J. Highly foldable and leakage-free electrodes enabled by ultrathin liquid metal micromeshes. *npj. Flex. Electron.* **2025**, *10*, 10. DOI
37. Song, J.; Seo, J.; Han, J.; Lee, J.; Lee, B. J. Ultrahigh emissivity of grating-patterned PDMS film from 8 to 13 μm wavelength regime. *Appl. Phys. Lett.* **2020**, *117*, 094101. DOI
38. Kim, J.; Kang, D.; Kwak, M. S.; et al. Ultrathin soft wearable sensor materials and structures: a review of current trends and prospectives. *ACS. Appl. Mater. Interfaces.* **2025**, *17*, 59994-60027. DOI PubMed PMC
39. Liu, M.; Sun, J.; Sun, Z.; et al. A review of microfluidic technologies for thermal management in flexible electronics. *Lab. Chip.* **2026**, *26*, 1417-43. DOI PubMed
40. Li, J.; Zhou, Y.; Jiang, C.; Lei, D.; Yu, X. Recent advances in passive cooling materials for thermal management in flexible electronics. *J. Mater. Chem. C.* **2024**, *12*, 12179-206. DOI

41. Kim, K. B.; Baek, H. J. Photoplethysmography in wearable devices: a comprehensive review of technological advances, current challenges, and future directions. *Electronics* **2023**, *12*, 2923. DOI
42. Kazem, N.; Hellebrekers, T.; Majidi, C. Soft multifunctional composites and emulsions with liquid metals. *Adv. Mater.* **2017**, *29*, 1605985. DOI PubMed
43. Haque, A. B. M. T.; Tutika, R.; Byrum, R. L.; Bartlett, M. D. Programmable liquid metal microstructures for multifunctional soft thermal composites. *Adv. Funct. Mater.* **2020**, *30*, 2000832. DOI
44. Chen, J.; Wang, J.; Wang, S.; et al. High-stretchable and thermally conductive elastomeric composites for heat dissipation in flexible electronics. *ACS. Appl. Polym. Mater.* **2025**, *7*, 1784-94. DOI
45. Lee, G. H.; Kang, H.; Chung, J. W.; et al. Stretchable PPG sensor with light polarization for physical activity-permissible monitoring. *Sci. Adv.* **2022**, *8*, eabm3622. DOI PubMed PMC
46. Lou, Z.; Tao, J.; Wei, B.; et al. Near-infrared organic photodetectors toward skin-integrated photoplethysmography-electrocardiography multimodal sensing system. *Adv. Sci.* **2023**, *10*, 2304174. DOI PubMed PMC